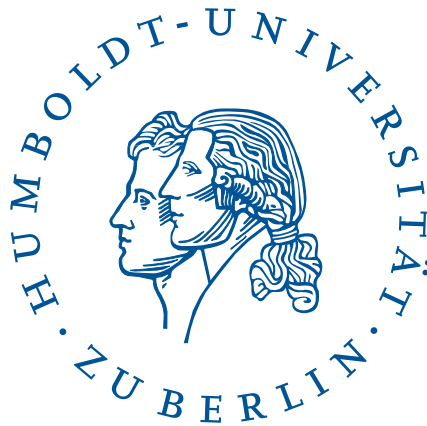


# Transient-Searches for eROSITA: Performance-Studies

## BACHELORARBEIT

zur Erlangung des akademischen Grades  
Bachelor of Science  
(B. Sc.)  
im Fach Physik



eingereicht an der  
Mathematisch-Naturwissenschaftlichen Fakultät I  
Institut für Physik  
Humboldt-Universität zu Berlin

von  
Herrn Andreas Berberich  
geboren am 17.12.1991 in Miltenberg

Betreuung:

1. *Prof. Dr. Thomas Lohse*
2. *Prof. Dr. Jörn Wilms (FAU Erlangen-Nürnberg)*

eingereicht am: *07. März 2016*

## **Abstract**

In this bachelor thesis it is about a performance study for eROSITA, a X-ray telescope scheduled to be launched in 2017. More precisely, an assessment for eROSITA's ability to detect transient sources is made. After giving information about the eROSITA mission and transients in general, a SIMPUT catalogue used as simulation input is explained and created. Afterwards, the simulation is evaluated. Therefore, the particular source counts are compared with the corresponding background counts to make an assessment how many sources can be detected with a high significance. Subsequently, a comparison of the input and output is made concerning the measured rates and light curves. Finally, an outlook for further and more detailed researches about this subject is given.

# Contents

<b>1</b>	<b>Introduction</b>	<b>2</b>
1.1	Motivation . . . . .	2
1.2	The eROSITA All Sky Survey . . . . .	2
1.3	Technical details . . . . .	3
<b>2</b>	<b>Transient X-ray Sources</b>	<b>6</b>
2.1	X-ray binaries . . . . .	7
2.2	The Crab Nebula . . . . .	9
<b>3</b>	<b>The simulation</b>	<b>10</b>
3.1	The SIXTE software . . . . .	10
3.2	Simulation input . . . . .	10
3.2.1	Source catalogue . . . . .	10
3.2.2	RXTE's All Sky Monitor (ASM) . . . . .	11
3.2.3	The background . . . . .	11
3.2.4	eROSITA's attitude . . . . .	12
3.3	The imaging process . . . . .	12
3.3.1	Vignetting Function . . . . .	12
3.3.2	Point Spread Function (PSF) . . . . .	13
3.3.3	Ancillary Response Function (ARF) . . . . .	14
3.4	The detector measuring process . . . . .	14
3.4.1	Redistribution Matrix File (RMF) . . . . .	14
3.4.2	Split events . . . . .	15
3.4.3	Pileup . . . . .	15
3.5	Photon creation in SIXTE . . . . .	15
<b>4</b>	<b>Results</b>	<b>17</b>
4.1	Results of the simulation . . . . .	18
4.1.1	Background . . . . .	19
4.1.2	Light curve extraction . . . . .	20
4.1.3	Comparison between the ASM- and eROSITA counts . . . . .	22
4.2	Discussion . . . . .	24

# List of Figures

1.1	SRG-satellite . . . . .	3
1.2	Scanning methode . . . . .	3
1.3	Visualisation of the exposure time . . . . .	4
1.4	Lagrangian points . . . . .	4
2.1	The Cyg X-1 binary system . . . . .	7
2.2	The Crab Nebula . . . . .	9
3.1	Simulated detector data . . . . .	12
3.2	eROSITA's vignetting function . . . . .	13
3.3	eROSITA's PSF . . . . .	14
3.4	eROSITA's ARF . . . . .	14
3.5	Photon process routine . . . . .	16
4.1	The energy spectral shape used for the simulation input . . . . .	18
4.2	Visualisation of the all sky survey . . . . .	19
4.3	The detektor light curve . . . . .	20
4.4	Total source counts . . . . .	21
4.5	Comparison between ASM and eROSITA rates . . . . .	23
4.6	Comparison between input and output light curves of the source IGRJ17098-3626 . . . . .	24

# List of Tables

1.1	Specifications of eROSITA . . . . .	5
3.1	Specifications of the ASM . . . . .	11
4.1	The background counts . . . . .	20
4.2	Pairs of data . . . . .	23

# Chapter 1

## Introduction

The Extended ROentgen Survey with an Imaging Telescope Array (eROSITA) is a X-ray telescope scheduled to be launched in 2017 from Baikonur. Together with the Russian Astronomical Roentgen Telescope (ART) eROSITA will be one of two instruments aboard the Russian Spectrum-Roentgen-Gamma satellite (SRG, Fig. 1.1<sup>1</sup>). The development of eROSITA is distributed to several institutes, including the Remeis-Sternwarte in Bamberg. The construction is led by the Max-Planck-Institute for Extraterrestrial Physics (MPE) in Munich.

### 1.1 Motivation

The aim of the eROSITA mission are measurements to study current cosmological models (Predehl et al., 2006). Amongst other things it is planned to test the dark energy model, study the large scale structure of the universe, and research the evolution of black holes. To achieve these goals eROSITA has to detect from 50000 to 100000 galaxy clusters, which are detectable by the radiation of the hot intergalactic gas in the centre of these clusters. By comparison of nearby (i.e., old) and distant (i.e., young) Active Galactic Nucleus (AGNs) believed to be massive black holes in the centre of galaxies, measurements of the evolution of black holes are realised. In order to detect the demanded number of objects, eROSITA's sensitivity has to be improved compared to the precursor missions such as ROSAT.

### 1.2 The eROSITA All Sky Survey

eROSITA will perform a four year all sky survey. During the survey one full image of the sky will take half a year. Thus each part of the sky will be revisited for at least 8 times. Afterwards it is planned to carry out pointed observations for several years. eROSITA will scan the sky in great circles (Fig. 1.2), of which each takes four hours. As the satellite will be placed in L2 (Fig 1.4<sup>2</sup>) and the earth moves around the sun, the circles move by  $1^\circ$  per day. The consequence of this scanning method is a wide survey of the whole sky and a deep survey near the Poles of the SRG orbit, as the telescopes point to the poles direction more often. The poles are located at

---

<sup>1</sup>[http://www.unituebingen.de/fileadmin/\\_migrated/RTE/RTEmagicC\\_eROSITA\\_satellite\\_02.jpg](http://www.unituebingen.de/fileadmin/_migrated/RTE/RTEmagicC_eROSITA_satellite_02.jpg)

<sup>2</sup>[https://upload.wikimedia.org/wikipedia/commons/5/5f/Lagrangian\\_points\\_equipotential.jpg](https://upload.wikimedia.org/wikipedia/commons/5/5f/Lagrangian_points_equipotential.jpg)

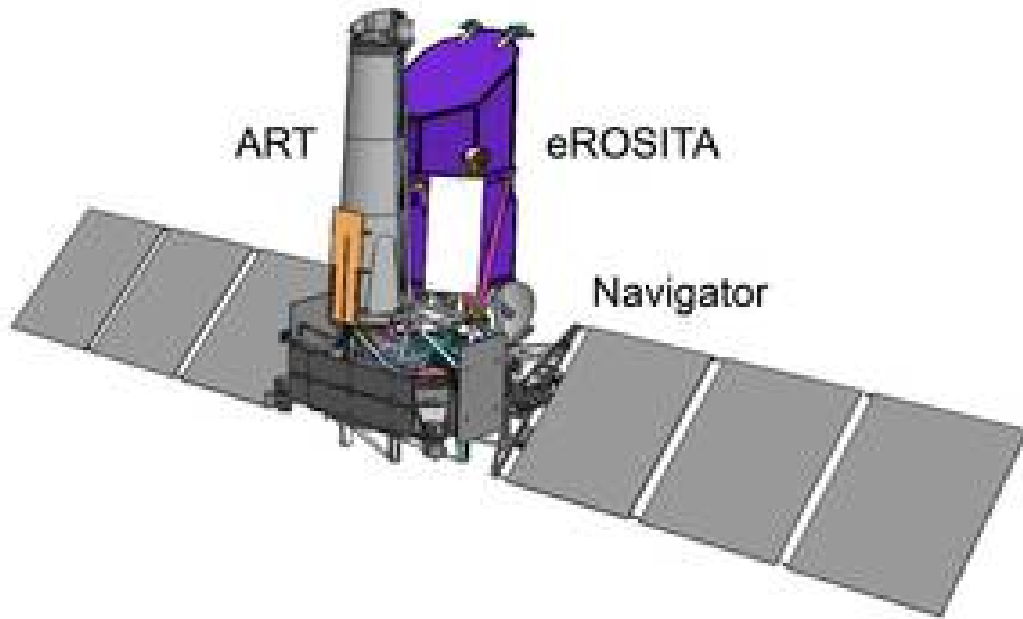


Figure 1.1: eROSITA and ART aboard the SRG-satellite with its navigator platform

about  $RA = 270.00^\circ$  and  $DEC = 66.20^\circ$  and about  $RA = 90.0^\circ$  and  $DEC = -66.20^\circ$ , respectively. Figure 1.3 visualizes the exposure time in the respective area of the sky. Therefore one compute the time eROSITA points towards the particular direction and assigns each pixel its exposure time. The brighter the spot the more exposure time. The image is scaled logarithmically due to the big differences between the exposure time at the poles compared to the rest of the sky.

### 1.3 Technical details

eROSITA is the the descendant of the ABRIXAS mission (A BRoadband Imaging X-ray All-sky Survey), which failed in 1999. In order to satisfy the more stringent

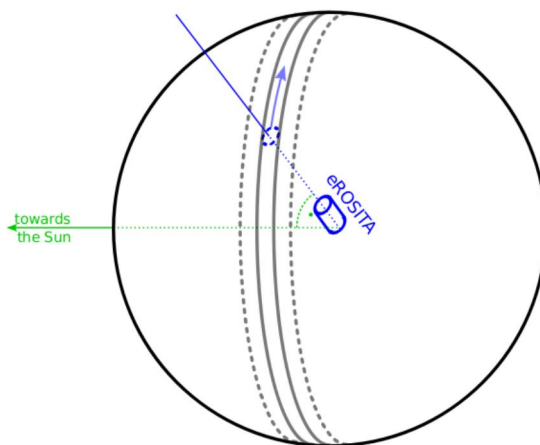


Figure 1.2: eROSITA's attitude to scan the sky; taken from (Friedrich, 2013)

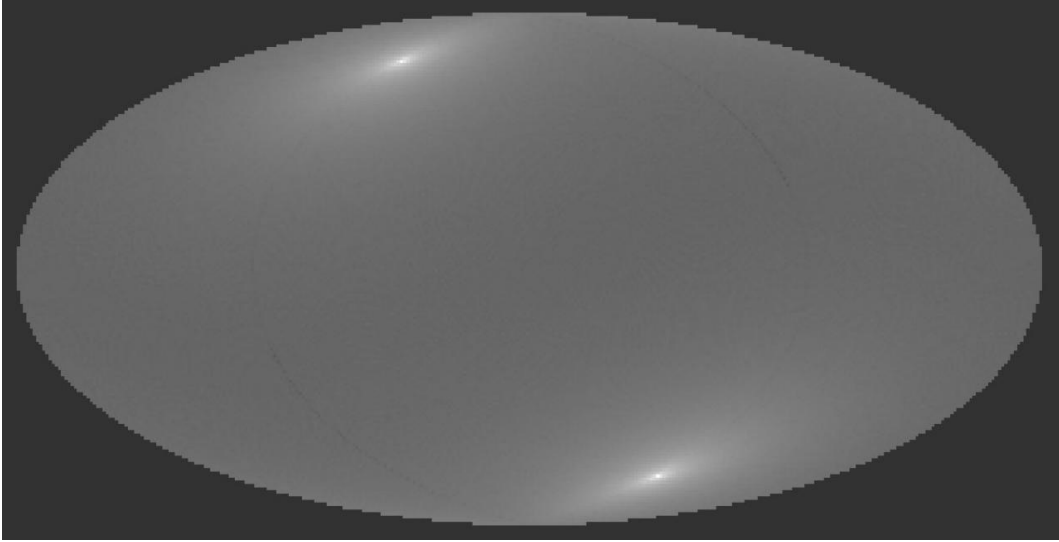


Figure 1.3: Logarithmic visualisation of eROSITA's exposure time for one all sky survey lasting 15768000 seconds.

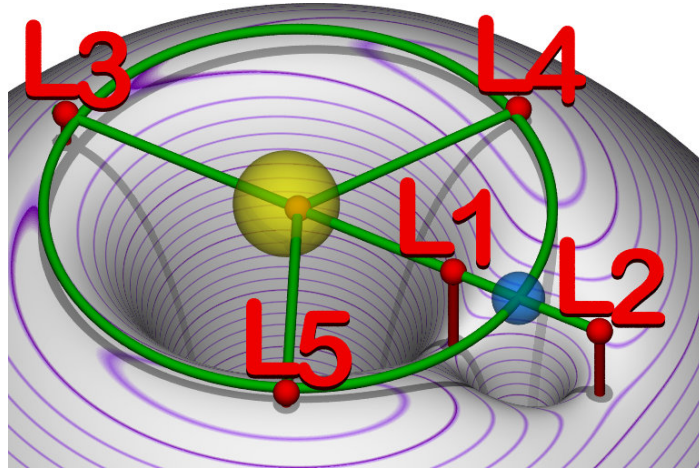


Figure 1.4: The Lagrangian points of the earth-sun-system

requirements for eROSITA, the optics had to be improved (Predehl et al., 2006). eROSITA consists of seven Wolter-I mirror modules (Wolter, 1952) in a hexagonal arrangement with 54 mirror shells each. As mentioned before, it will be placed in the Lagrangian Point L2 (Fig. 1.4). The telescope's energy range is from 0.2 keV to 10 keV with an energy-dependent sensitivity, e.g., the resolution at 6 keV is about 130 keV. eROSITA will collect data with a field of view (FOV) diameter of about 61 arcsec. Its spatial resolution depends on the energy and the off-axis angle due to the telescope's geometry and mirror properties. At 1 keV the angular resolution is circa 15 arcsec on-axis and 28 arcsec averaged over the field of view. A detailed discussion about the energy- and off-axis dependence will be given in Sect. 3.3 and 3.4. In order to avoid out of time events, the time resolution was improved to 50 ms. Out of time events are photons arriving during readout. The pixel size was reduced to  $75 \mu\text{m} \times 75 \mu\text{m}$  divided up into  $256 \times 256$  pixels. The technical details are summarized in Table 1.1.

Table 1.1: eROSITA's specifications (Predehl, 2012)

number of tubes/detectors	7
mirror shells per module	54
focal length	1.6 metres
diameter seen from the front	36 cm
size of pixels	$75 \mu \times 75 \mu\text{m}$
detector pixels	384 x 384
field of view	61 arcmin
on-axis resolution	15 arcsec at 1 keV
energy range	0.2 - 10 keV
energy resolution	$\approx 130 \text{ eV}$ at 6 keV
time resolution	$50 \mu\text{m}$
detector	pn-CCD cameras
operating temperature	- 80°

# Chapter 2

## Transient X-ray Sources

An astronomical X-ray source in general is defined as an astronomical object or system, which emits electromagnetic radiation with photon energies from about 1 eV to several hundreds of eV. Each source has a more or less time-dependent luminosity defined as the total energy emitted by the particular source caused by complex inner processes. In order to perform further studies, a light curve is created for each source generated out of the data various telescopes provide. A light curve is a graph of light intensity within a particular energy interval dependent on the properties of the telescope. Each telescope is sensitive within its own energy band. For example eROSITA is sensitive for energies from 0.2 to 10 keV (Sect. 1.3). The unit of a light curve is given in counts per seconds or energy per time. Transient sources, which this thesis is about, are characterised by a time dependent luminosity, which varies by up to several magnitudes within specific periods of time. There are different kinds of transients, classified by the actual occurring phenomenon leading to radiation. Often a further classification regarding, luminosity, periodicity and, time variability can be made. Some transient sources only occur during one fixed period of time, which can last from seconds to several years, for example Gamma Ray Bursts or Tidal Disruption Events. Other transients have a clear pattern with a constant luminosity periodically interrupted by huge outbursts. These outbursts can occur every few hours, days or even years. On the other hand some transients show pulsations in time periods of seconds or even milliseconds. Another time-dependent property of transients that must be mentioned is their spectrum. A spectrum is defined as the number of emitted photons dependent on their energies. This thesis and especially the simulation input (Sect. 3.2.1) and evaluation (Sect. 4) is focused on the time-dependence of the luminosity. A special priority is set on binaries (Sect. 2.1), astronomical systems consisting of two or more interacting objects, as these are the brightest X-ray sources in the sky. Due to eROSITA's special scanning method and small field of view (Sect. 1) in combination with the time-dependent luminosity of transients, eROSITA will not be able to detect all transients. In other words eROSITA has to point to the right spot at the right time to detect transient sources. In this thesis an assessment about eROSITA's performance regarding the detection of time-dependent sources will be made. Special attention will be given to the assessment of how many bright transients eROSITA will be able to detect. But first, some information about binaries in general is given (Sect. 2.1) and one important X-ray source is outlined (Sect. 2.2).

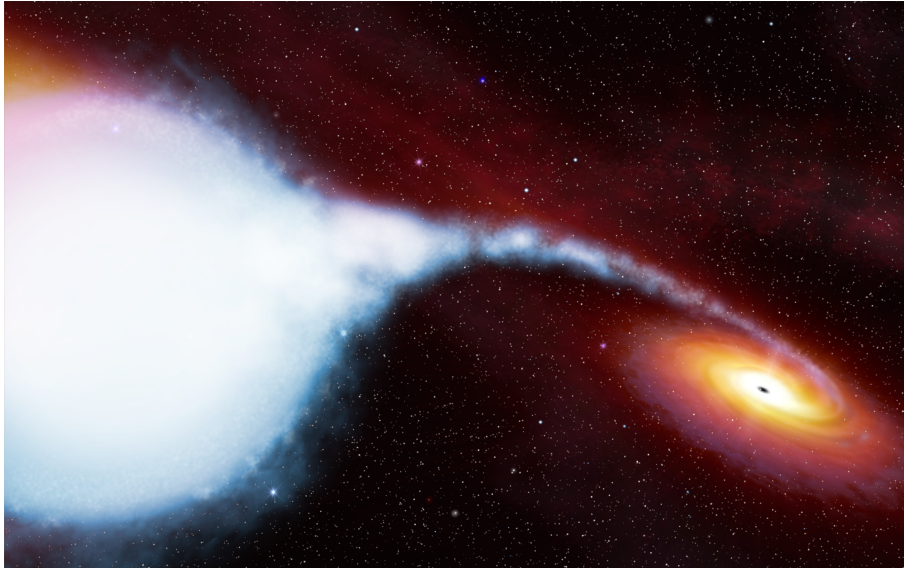


Figure 2.1: Artistical visualisation of the black hole binary system Cyg X-1

## 2.1 X-ray binaries

Binaries in general consist of two or more astronomical objects, which interact with each other. The following is only about systems composed of two objects consisting of an accretor and a donor. The accretor is a compact object with high density and can be either a neutron star, black hole or white dwarf. The donor is a normal star, which can vary from system to system regarding its mass and luminosity. Fig. 2.1 <sup>1</sup> shows an artistic visualisation of a black hole binary. More precisely, it is the Cyg X-1 system, probably consisting of a black hole and an O-star (Nowak et al., 2012). What all binary systems have in common is the fundamental phenomenon which leads to radiation. Due to its immense density and the resulting gravitational potential the accretor accretes material provided by the donor. This accreted matter is constrained into an accretion disc around the compact object, wherein the material is heated due to gravitational and frictional forces. This heated material emits the X-ray radiation, which is observed with the telescopes and is the basis for further studies like, e.g., spectroscopy. Before giving more information about binaries, the three phenomenons responsible for accretion are discussed:

### Wind-fed systems

The companion, mostly a high mass O- or B- star (Mauche et al., 2008), has got a powerful wind which blows matter away from the star's surface. This wind is so powerful that there is sufficient material being lost in all directions and thus the compact object can accrete enough matter providing sufficient energy and leading to massive X-ray emission.

### Roche-lobe overflow

The companion, mostly a low mass star (Savonije, 1978), expands until it fills its Roche-lobe and oversteps the Lagrangian Point L1 (Fig. 1.4). The consequence is a flow of material from the companion to its compact object and the formation of an accretion disc.

---

<sup>1</sup>[https://de.wikipedia.org/wiki/R%C3%B6tgendoppelstern#/media/File:Cygnus\\_X-1.png](https://de.wikipedia.org/wiki/R%C3%B6tgendoppelstern#/media/File:Cygnus_X-1.png)

## Be-disc transfer

Be stars often form a material disc around themselves (Harding, 2013). In case of a small distance between the accretor and the star (e.g., during periastron) the accretor can accrete material from the star's disc.

As mentioned before, you can often observe X-ray pulsations in time intervals from milliseconds to seconds, which can only be caused by the spin of the compact object, as some of these pulsations are exactly periodic. In a stable object the centrifugal force felt on the surface must not be higher than the gravitational force. This fact allows conclusions about the density of the particular compact object and therefore the type of the accretor can be determined, as their density varies between different objects. In comparison, binaries consisting of a white dwarf, called cataclysmic variable stars, are less luminous due to their less density (Seward & Charles, 1995). Neutron star and black hole binaries can have luminosities up to  $10^{38}$  erg per second (Seward & Charles, 1995). An erg is  $0.1 \mu\text{J}$ . Thus it is straightforward to distinguish between cataclysmic variable stars and binaries consisting of a black hole or neutron star. However the distinction between a black hole and a neutron star is more complicated. Due to the fact that cataclysmic variable stars are less luminous, the focus is on binaries consisting of black holes or neutron stars in the following.

Both black holes and neutron stars arise from supernovas, when a star is collapsing at the end of its lifetime. Depending on the star's mass a black hole or a neutron star develops. If the star's mass is between 1.44 and 3 solar masses a neutron star will occur. Due to the spin research discussed before, the radius of a neutron star can be estimated to 10 kilometres. Its density is from about  $10^{14} \frac{\text{g}}{\text{cm}^3}$  to probably  $10^{15} \frac{\text{g}}{\text{cm}^3}$  at the centre (Seward & Charles, 1995). This leads to a gravitational force at the surface, which is  $10^{11}$  times higher than on earth with the consequence that each solid object is disrupted when it comes close to the neutron star (A. van Riper & Epstein, 1993). Furthermore, neutron stars have powerful magnetic fields, which tear electrons from the surface and accelerate them, resulting in electro magnetic radiation. Therefore you can see the pulsations when one magnetic pole rotates through the observer's line of view.

Stars with masses higher than 3 solar masses generate a black hole when collapsing. Black holes are object with an immensely high density and high gravitational potential. This potential is so immense that there is an area around black holes, wherein any particles including photons are absorbed. This area is called the event horizon and only assumptions about the area within this horizon can be made.

As discussed before, binaries show characteristic variabilities from milliseconds to months or even years resulting in various different classifications. On the one hand there are systems, which are understood quite well, whereas on the other side there are still systems, which bring up many questions. In order to get detailed information about the specific types of binaries, it is, e.g., referred to Seward & Charles (1995).

Nevertheless, several aspects which can be crucial for the particular time-dependent variability regarding luminosity, should be mentioned.

The first aspect, which can be crucial for the occurring pattern, is the precession of the accretor, its accretion disc or the companion. Moreover, the companion's wind or its mass loss rate in general can vary. Furthermore, the spin behaviour of the compact object can change. In the case of a change in its spin period the periodicity of the pulsations would change too. In addition, a tilted accretion disc, as the observation depends on the perspective, and a variation of the magnetic field,

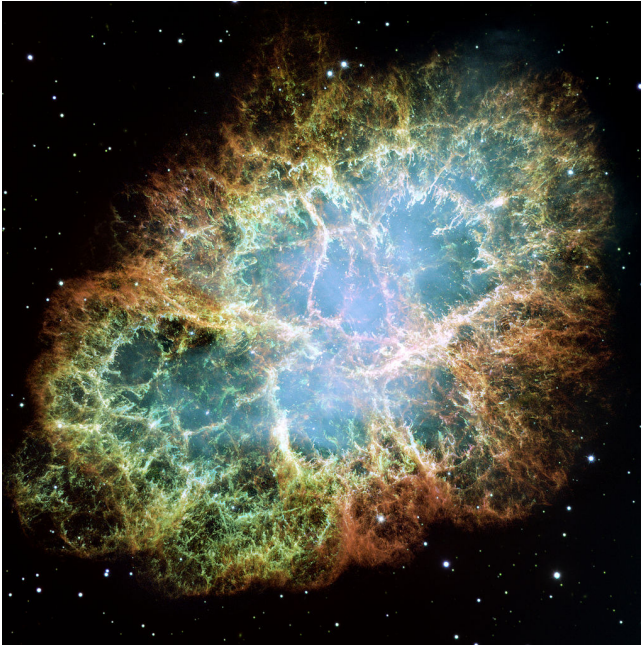


Figure 2.2: The Crab Nebula. The image was taken by NASA's Hubble Space Telescope.

influences the luminosity. Finally the mass density in the accretion disc has an impact on the luminosity. If the accretion disc density exceed a particular value, this will result in reabsorption of the photons and therefore decreased intensity of the emitted radiation.

## 2.2 The Crab Nebula

The Crab Nebula is one of the brightest sources in the X-ray sky with a right ascension (RA) of  $83.633^\circ$  and a declination (DEC) of  $22.014^\circ$ . The Crab Nebula is categorized as a supernova remnant with a distance from the earth of about 6500 light years. The pulsar located at the center of the Crab Nebula is likely a neutron star with 30 km in diameter. It has about one solar mass, however it produces 75000 more energy than the sun. The Crab Nebula's luminosity is almost constant with a flux of  $1.3 \cdot 10^{37}$  erg per second in the energy range from 0.5 to 8 keV (Mori et al., 2004). Due to the roughly time-independent electromagnetic radiation, it is both used as a unit for the flux and for calibration at the beginning of a telescope mission. In actuality, the crab nebula is slightly time-dependent, as there is a pulsar in its centre rotating about 30 times per second. Figure 2.2 <sup>2</sup> shows a picture of the Crab Nebula taken by NASA's Hubble Space Telescope.

---

<sup>2</sup>[https://en.wikipedia.org/wiki/Crab\\_Nebula#/media/File:Crab\\_Nebula.jpg](https://en.wikipedia.org/wiki/Crab_Nebula#/media/File:Crab_Nebula.jpg)

# Chapter 3

## The simulation

### 3.1 The SIXTE software

Simulation of X-ray Telescopes (SIXTE) is a software package developed at the Erlangen Centre for Astroparticle Physics (ECAP) (Schmid (2008) and Schmid (2012)). The simulation, which will be evaluated in this thesis, is done with SIXTE. More specifically the tool `runsixt` was used to simulate eROSITA's all sky survey. The concept of the simulation is related to the real measurement process of a telescope. The fundamental principle of the simulation is the creation of a photon list, wherein each arriving photon is listed with its position, arriving time, and energy. But before dealing with the concrete loop SIXTE performs in order to create a photon list (Sect. 3.5), there is given information about other aspects of the simulation. At first, it is about the simulation input (Sect. 3.2), in which amongst other things information about the sources, which will be simulated, is given. Afterwards, Sect. 3.3 and 3.4 deal with the telescope- and detector-dependent effects, which have to be taken into account for real measurements and therefore for the simulation.

### 3.2 Simulation input

#### 3.2.1 Source catalogue

As mentioned before, SIXTE needs information about the sources, which are simulated. This is assured with a SIMulation inPUT (SIMPUT) catalogue file containing the necessary information. The SIMPUT file is based on the FITS file format (Pence et al., 2010), which is usually used in X-ray astronomy. The SIMPUT catalogue is created with data, a former mission provided. In this case the data of the All Sky Monitor (ASM) (Sect. 3.2.2) are taken. The SIMPUT file consists of different Header and Data Units (HDUs) containing the particular data and information. The core of the SIMPUT catalogue is the source catalogue (SRC\_CAT) HDU including amongst other things:

- **Source ID** Each source is listed with its ID
- **Name of the source** Each source is mentioned with its particular name
- **Position** Each particular position is given with its RA and its DEC
- **Spectrum** Each source is linked to its corresponding spectrum stored in a different HDU

Table 3.1: Specifications of the ASM

number of detectors	3
energy range	2 - 10 keV
sensitivity	20 mCrab = $4.8 \cdot 10^{-10}$ erg/s/cm <sup>2</sup>
field of view of each camera	$6 \times 90$ degrees
spatial resolution	$3' \times 15'$
time resolution	90 seconds

- **Light curve** Each source is linked to its particular light curve stored in a different HDU

A detailed description about the procedure performed, in order to create the SIMPUT catalogue, is given in Sect. 4.

### 3.2.2 RXTE's All Sky Monitor (ASM)

In order to get an idea about the properties of the data used for the SIMPUT catalogue, one has to be concerned with the mission, which provided these data. The Rossi X-Ray Timing Explorer (RXTE) was a satellite launched on December 30, 1995 from NASA's Kennedy Space Center and was placed in an orbit at an altitude of 580 km with an inclination of about 23 degrees (Lochner & Remillard, 1995). In total the RXTE was equipped with 3 astronomical instruments. First to be mentioned is the ASM, as its data are used as simulation input. The remaining instruments were the Proportional Counter Array (PCA), which measured low energies from 2 to 60 keV, and the High Energy X-ray Timing Experiment (HEXTE) used for higher energies from 15 to 250 keV (Giles et al., 1995). The ASM consists of three Shadow Cameras which were positioned to cover 70 % of the whole sky every time the instruments rotated by 360 degrees. One rotation was performed in 90 minutes with fixed position measurements for 90 seconds each, before the direction of pointing was changed. The received data are available in a source catalogue (<https://heasarc.gsfc.nasa.gov/docs/xte/ASM/sources.html>), wherein every source the ASM detected is listed with its light curve and position in the sky. A summary about the properties of the data the ASM generated are given in table 3.1.

### 3.2.3 The background

In order to make the simulation as realistic as possible, the cosmic particle background and the cosmic X-ray background has to be considered. Photons emitted by the cosmic X-ray background or other charged particles belonging to the cosmic particle background are detected just like photons emitted from sources of the SIMPUT catalogue. In the simulation, the cosmic X-ray background is implemented by adding many new faint sources to the SRC\_CAT, corresponding to the flux distribution based on earlier X-ray missions (Schmid, 2012). The cosmic particle background is considered with a FITS file containing a hit list of background particles like electrons or protons. This FITS file is obtained from a simulation performed by Tenzer et al. (2010), see also (Schmid, 2012). The detector can not differ between photons and these charged particles, as it just measures the charge cloud caused by arriving particles or photons. In the analysis of the simulation (Sect. 4) these background

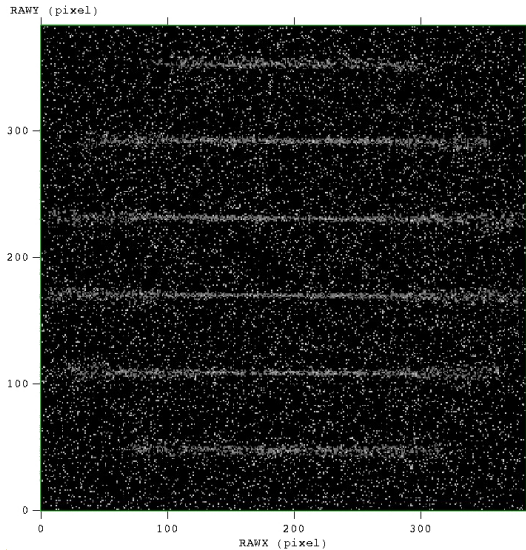


Figure 3.1: Simulated data of a constant 30 mCrab source with eROSITA’s attitude. The characteristic detector image shows stripes at the positions the source is detected on the focal plane for subsequent rotates of the spacecraft. In total, the source is detectable for 6 times.

events will be discussed more precisely. Furthermore, an assessment will be made to compare these background events with the photons emitted by the sources.

### 3.2.4 eROSITA’s attitude

The attitude is defined as the direction the telescopes point at a particular time. For the simulation the attitude is described in a file containing time, right ascension, and declination. The time resolution is 60 seconds. For the simulation a linear interpolation between two data points is performed. Due to the particular scanning method (Sect. 1.2), a characteristic detector image develops (Fig. 3.1). Each source is seen with its particular streaks as it moves through the detector’s field of view. Each run lasts from about 25 seconds at the edge to 60 seconds in the centre. The number of stripes, which can be seen, depends on the source’s position in the sky. If the source is near the poles of the SRG orbit, it will be seen more often than at the equator. Each source will be seen at least 6 times, if it is bright enough to be detected. Fig. 3.1 shows a constant 30 mCrab source near the equator, which is detected well for 6 times separated by 4 hours, the time required for one great circle (Sect. 1.2).

## 3.3 The imaging process

The properties and quality of the measurements depend, amongst other things, on the construction of the telescope. Therefore the specific properties of the optics are taken into account. For eROSITA the characteristics of Wolter-I mirror modules are crucial. Some of the effects decisive for the quality of the data the telescope provides have to be considered and implemented in the simulation. Detailed information about the individual effect and the implementation can not be given in this thesis but can be found in Schmid (2008) and Schmid (2012).

### 3.3.1 Vignetting Function

At first, both the off-axis angle and the azimuth angle are determined with the telescope’s attitude and the particular photon direction of origin. If the photon is

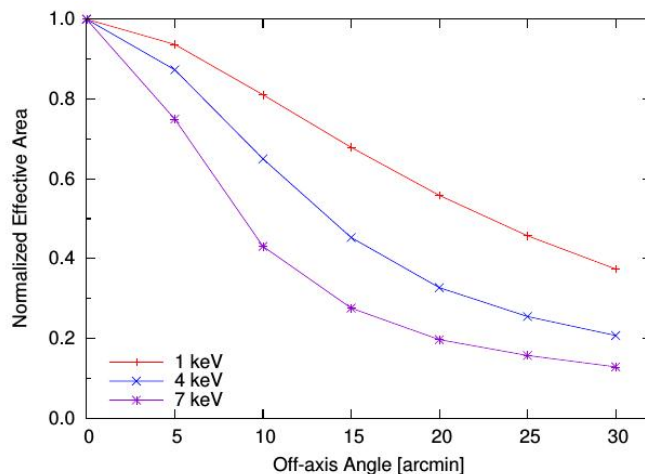


Figure 3.2: The vignetting function of eROSITA for different energies; taken from Friedrich (2013)

outside the FOV, it just will be rejected. For photons which are inside the FOV, the vignetting function (depending on the off-axis angle, the azimuth angle, and the photon's energy) characterises the probability that the photon is reflected correctly by the mirror shells of the telescope (Schmid, 2012). Correctly means that the incoming photon is actually hitting the surface of the detector. Therefore the vignetting function is the probability that the photon inside the FOV is actually hitting the detector's surface. Ideally the vignetting function would be equal one for each photon but in reality it has an value between zero and one, as not all photons, which are inside the FOV, actually hit the surface of the detector. Figure 3.2 shows the vignetting function of eROSITA for different energies. The dependence on the azimuth angle is neglected in this Figure.

### 3.3.2 Point Spread Function (PSF)

The PSF of an optical instrument describes its ability to image point-like sources. More specifically the PSF characterises the possibility to distinguish between point-like sources, due to the smearing of the imaging process. If two point-like sources are too close to each other the detector will only see one source, as photons from a point-like source are not imaged in exactly one detector pixel, due to the fact that there are several pixel wherein there is a probability that the photon arrives. The PSF depends on the off-axis angle and the energy of the photon (Schmid, 2008). This effect can be seen in Fig. 3.1, in which the spreading of the pixels occur at the edge of the detector. This spreading is caused by the astigmatism of the Wolter-I telescope. Thus the PSF is increasing for higher off-axis angles. The PSF is specified as the Half Width Energy (HEW), which defines the spreading of a point-like source. As the whole FOV of eROSITA is used to optimise the sensitivity, high off-axis angles and their consequence must be considered. For eROSITA the HEW is between 15 arcsec on-axis and 28 arcsec off-axis (Predehl, 2012). Fig. 3.3 shows the PSF for different off-axis angles and energies. To be more exact, you have to consider that the azimuthal angle affects the PSF too, which is neglected here.

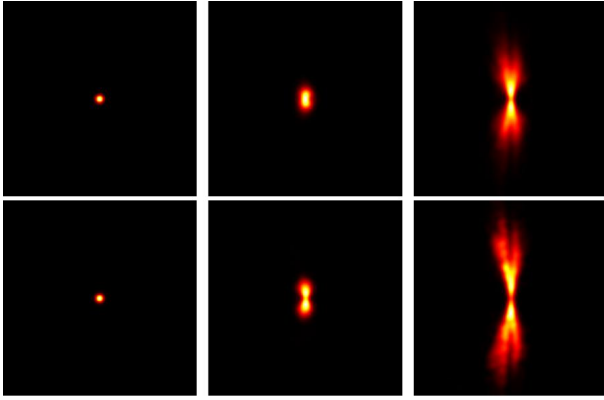


Figure 3.3: eROSITA’s PSF for different off-axis angles (0, 15 and 30 arcmin) and different energies (first row: 4 keV, second row: 7 keV); taken from Schmid (2012)

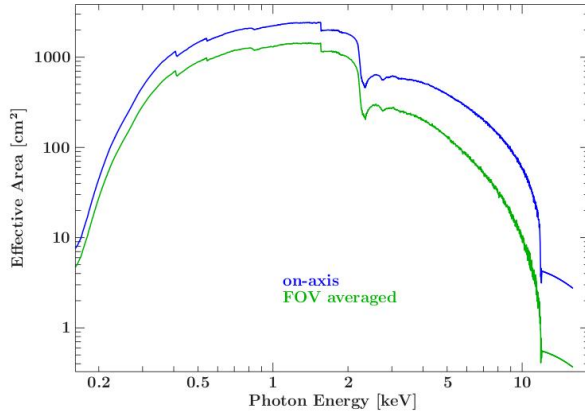


Figure 3.4: eROSITA’s ARF. It is shown the on-axis ARF (blue) and the FOV averaged (green); taken from Friedrich (2013)

### 3.3.3 Ancillary Response Function (ARF)

Each X-ray mirror system has an effective area defined as the efficiency to collect photons. In order to achieve the aims mentioned in Sect. 1.1, a high effective area resulting in a high sensitivity is needed. The ARF is defined as the product of the projected on axis area with the reflectivity of the mirrors. As the critical angle for total reflection, thus the probability that the photons can be detected, decreases for higher energies (Schmid, 2012), the ARF is energy dependent. In order to optimise the reflectivity of the mirror system, eROSITA is equipped with 54 mirrors shells (Sect. 1.3). The ARF is often combined with other instrumental effects, e.g., the quantum efficiency, which defines the probability that a photon hitting the surface of the detector is actually detected. Figure 3.4 shows both the on-axis ARF and the FOV averaged ARF of eROSITA.

## 3.4 The detector measuring process

As we already discussed the consequences of the telescope’s optics, it is about the effects caused by the detector now. The fundamental principle of the used CCD detector is to measure the charge cloud of arriving photons created in form of electron-hole pairs in the semiconductor material (Schmid, 2008). Therefore some important facts have to be mentioned.

### 3.4.1 Redistribution Matrix File (RMF)

Due to fluctuations caused by the Poisson distribution of the photoelectrons and potential systematic effects of the detector, the energy measured by the detector

will be different than the actual photon energy. This effect is worsened by the presence of electronic noise or incomplete conversion of the photon energy to electrical charge in the detector (Schmid, 2012). The RMF defines the probability density for the detection of an arriving photon with a particular energy in the respective energy channels of the detector. The ideal case of the RMF would be the identity matrix with the consequence that each photon is dedicated to its correct channel. Unfortunately, in reality there are entries unequal to zero besides the diagonal due to the finite resolution of the detector.

### 3.4.2 Split events

As mentioned before, incoming photons create a charge cloud in the detector. The higher the energy of the photon the higher the amount of electron-hole pairs. The charge clouds have a non zero width. If the photon is hitting the detector right between the border of two pixels, or if the energy is high enough to create a relatively wide charge cloud, it will be possible that the charge is detected in more than one pixel. If this happens one event is detected in several pixels. This is called split event. The software responsible for the evaluation of the data has to consider these events with the usage of a suitable algorithm (Schmid, 2012).

### 3.4.3 Pileup

Charges generated by incoming photons are not read out immediately. They are stored in the pixels during one read-out cycle, which lasts 50 ms (Sect. 3.5). For bright sources with a high quantity of arriving photons two or more photons could impinge on the same pixel during one read-out cycle. In this case the detector only measures the sum of the charge clouds generated by all incoming photons which is erroneously interpreted as one photon with a higher energy. As a consequence of this effect the measured count rate decreases and the particular spectrum is distorted. This has to be taken into account for the simulation to get realistic results (Schmid, 2008) and will be important for the analysis for bright sources later on (Sect. 4).

## 3.5 Photon creation in SIXTE

After dealing with the aspects, which have to be considered for the simulation, one can be concerned with the actual procedure SIXTE performs. As mentioned in Sect. 3.1, the primary aim is the creation of a photon list. Therefore, the SIMPUT catalogue (Sect. 3.2.1), the attitude file (Sect. 3.2.4), the XMLfile, containing all the information discussed in Sect. 3.3 and 3.4, and the total exposure time are handed over to SIXTE. In this case the exposure time is set to  $1.6 \cdot 10^7$  seconds, as this is slightly more than half a year to ensure that the whole exposure time is taken into account. In order to create the actual photon list, SIXTE performs the following tasks in a loop:

1. A pre-selection and check if the particular source is inside the FOV, according to the current pointing and motion of the telescope. The pre-selection is based on the positions stored in the SIMPUT catalogue (Sect. 3.2.1). If the source is inside the FOV, the following steps will be performed. Otherwise, the source will be neglected. This step is updated every 50 ms.

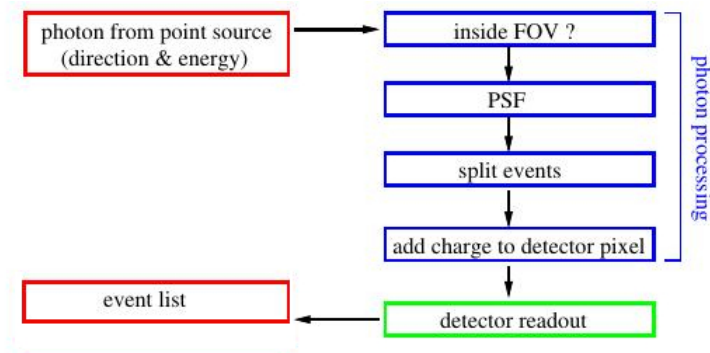


Figure 3.5: The photon process routine; taken from Schmid (2008)

2. The light curves of pre-selected sources, which are close to the FOV, are generated by using a special Monte Carlo algorithm. Due to the fact that there is only one data point every 90 seconds (Sect. 3.2.2), it is interpolated linearly between two data points.
3. The photons are generated for the selected source according to its light curve just created and the source's spectrum, which is stored in the SIMPUT catalogue too.
4. If the photon is emitted inside the FOV, the photon process routine will be performed (Fig. 3.5). Some photons can get lost due to the properties of the detector and telescope (Sect. 3.3 and 3.4).
5. The charge clouds, which are created by photons hitting the detector, are collected in the detector pixels during the read-out interval of 50 ms.
6. The translation from the charge clouds to the photon energies are made according to the RMF (Sect. 3.4.1).
7. Finally the event list is created, wherein the coordinates, time, and measured energies of the events are stored.

After the loop is finished, SIXTE filters the created event list and discards invalid events. These events are caused by split events (Sect. 3.4.2) for example. In the evaluation (Sect. 4) the filtered event file is used.

# Chapter 4

## Results

As mentioned in Sect. 3.2.1, the primary preparation, in order to perform an eROSITA all sky survey, was the creation of the SIMPUT catalogue. In the SIMPUT catalogue, the sources are serially numbered and their names and positions are taken out of the source catalogue mentioned in Sect. 3.2.2. The spectrum HDU, which every source is linked to, is simplified in this thesis. As mentioned in Sect. 2, each source has actually a more complex and time variable spectrum. However, in this thesis, a time-independent spectrum is assumed, which is the same for each source. It is defined as the product of a power law with a factor considering the absorption of the interstellar medium (Wilms, Allen & McCray, 2000). The power law has the form

$$A(E) = K \cdot E^{-\alpha} \quad (4.1)$$

in which  $K$  is a norm factor and  $\alpha$  is the photon index, set to 1.9 in the following, as this is a realistic value (Wilms, Allen & McCray, 2000). The absorption is given by

$$I_{\text{obs}}(E) = e^{-\sigma_{\text{ISM}}(E) \cdot N_{\text{H}}} I_{\text{source}}(E) \quad (4.2)$$

where  $I_{\text{obs}}(E)$  is the observed X-ray spectrum of a source,  $I_{\text{source}}(E)$  is the X-ray spectrum emitted by the source, and  $\sigma_{\text{ISM}}(E)$  is the total photo ionization cross Section of the inter stellar medium. The hydrogen equivalent column  $N_{\text{H}}$  is specified in atoms/cm<sup>2</sup> and is set to  $0.4 \cdot 10^{22}$  cm<sup>-2</sup>. The resulting spectrum is shown in Fig. 4.1, note that only its shape and not the absolute value is crucial for the simulation.

In contrast to the spectrum, each light curve is stored in a different HDU. As the light curves in the source catalogue used as input (Sect. 3.2.2) are defined during the time of the measurements of the ASM and the simulation for the eROSITA survey starts at the beginning of the eROSITA mission, the light curves have to be shifted in time. Unfortunately, the ASM light curves start at different times, as each light curve starts at the time when the ASM first detected the particular source. As the ASM could only cover 70 % of the sky, due to solar angle constraints, some sources were detected later on than others. Hence the light curves have to be shifted in time again, in order to guarantee that each light curve starts right before the beginning of eROSITA. Therefore both the starting time of each light curve and the latest starting time occurring are calculated. Afterwards, each light curve is postponed by this particular time. Two sources are excluded here because they have been detected only a few years after the start of the ASM mission. In order to guarantee that they are defined during the simulation, they are supplemented

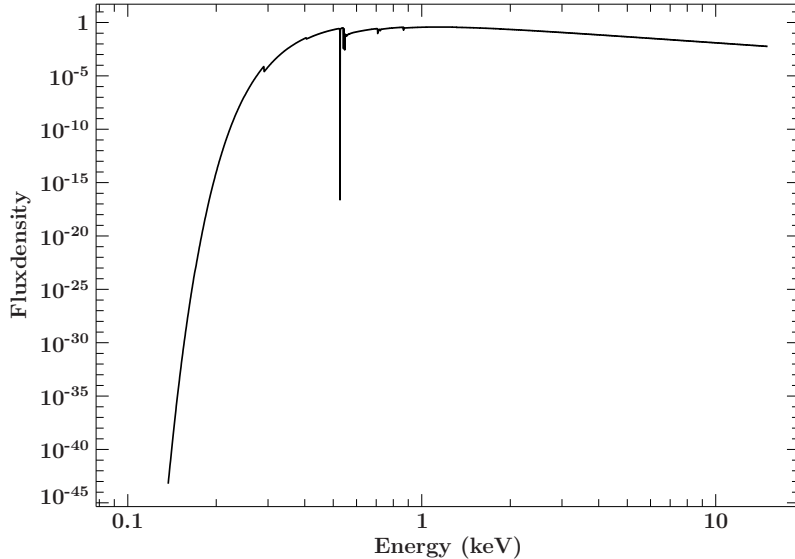


Figure 4.1: The energy spectral shape used in this thesis defined as the product of a power law with a factor responsible for the absorption  $A(E) \propto E^\alpha \cdot e^{-\sigma_{\text{ISM}}(E) \cdot N_{\text{H}}}$ . The photon index  $\alpha$  and  $N_{\text{H}}$  are set to 1.9 and  $0.4 \cdot 10^{22} \text{ cm}^{-2}$ , respectively.

with zeros. These 2 sources could have been discarded too. Finally, the light curves specified in counts per second are converted into units of Crab, where 0.075 counts/s equals to 1 mCrab for the ASM (Wen et al., 2006). The last step is made, as the counts per second specification is detector dependent, whereas the specification in Crab is detector independent. In total, there are 589 sources in the source catalogue.

## 4.1 Results of the simulation

As mentioned before, the simulation is used to create an event list, a FITS file, in which arriving and detected photons are listed with its time, positions and energies. This list is used for the following evaluation. But first of all the simulation is visualised with the tool `imgev`. In order to use `imgev`, one has to give over some input parameters, e.g., the event list, the amount of pixels with the corresponding intervals in which the declination and right ascension vary ( $-90^\circ$  -  $+90^\circ$  and  $0^\circ$  -  $360^\circ$ , respectively), and the file in which the image is stored. `Imgev` assigns each incoming photon its position in the sky. The brighter one pixel, the more incoming photons from the corresponding area of the sky. Fig. 4.2 shows the results of this tool. Basically, each bright pixel is a different source with the exception of the poles which are the two wide bright areas symmetrical to each other. There are more incoming photons at the poles compared to the rest of the source-free sky, due to the larger exposure time. This is the consequence of the background (Sect. 3.2.3) and must be considered later on (Sect. 4.1.1).

As each photon is stored with its arrival time, a total detector light curve can be created. Therefore the tool `makelc` is used. After handing over input parameters such as the event list, the output file, the length of the total light curve, and the time resolution, the tool generates a FITS file, wherein the time is binned in intervals and each photon is assigned to its particular interval. In this case  $1.6 \cdot 10^7$  seconds are set as total length, as this is the total exposure time in the simulation. The time resolution is set to 50 s. After adding a time column to the output file, which has

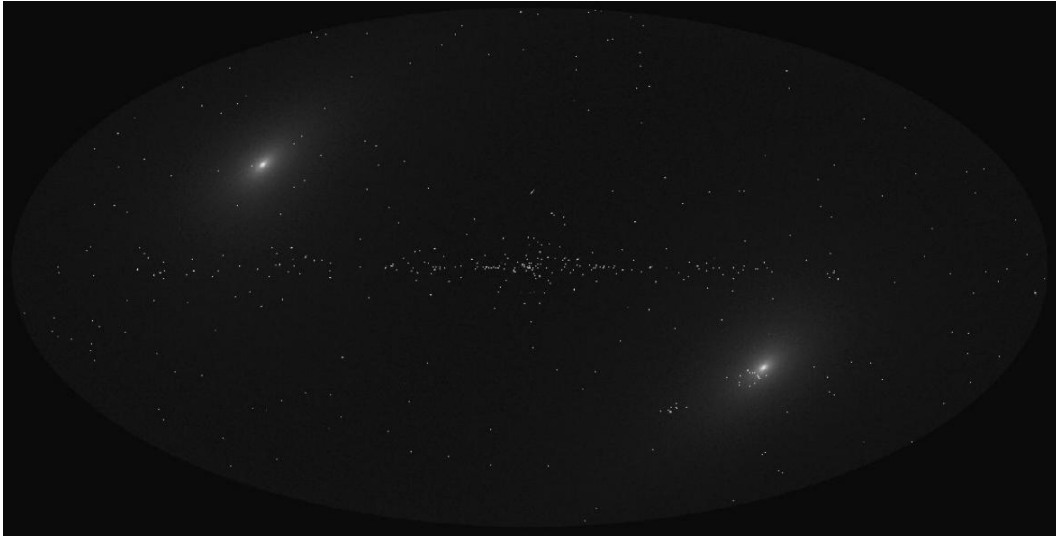


Figure 4.2: The image of the all sky survey. The brighter one pixel, the more incoming photons at the particular position. The two wide bright areas are the survey poles. Due to the large exposure time, many photons are detected. It is scaled logarithmic, due to the big differences between the pixels.

to be adapted to the specified time resolution, the light curve can be plotted. The output of this tool can be seen in Fig. 4.3, which shows that the detector count rate is strongly variable. This has consequences for the design of the Spectrum-x-Gamma telemetry system which has to accommodate the partially very high count rates.

#### 4.1.1 Background

As mentioned in Sect. 3.2.3, the background is taken into account in order to make the simulation as realistic as possible. Hence its influence on the data has to be analysed. This is especially crucial when it is about to find a criteria for the source detection (Sect. 4.1.2). There are two possibilities to give an assessment for the background rate. At first, an all sky survey without any sources can be performed. The background rate  $c_b$  is calculated by dividing the total counts  $C$  by the total exposure time  $T_{\text{Exp}}$ . In the following  $c_x$  is the rate of the parameter abbreviated with x and  $C_y$  is the total number of counts of the parameter abbreviated with y. The second possibility, which is performed here, is the examination of 1000 random positions, where no source is present. Each photon which is detected within a certain area around the particular position is counted by checking each event of the event list. A good selection for the size of this area is in the same magnitude of the PSF, as this defines the area a point-like source can spread on the detector (3.3.2). In order to give a maximum assessment, the area was defined as a circle around the particular position with a radius of 40 arcsec, which is slightly more than the PSF. Table 4.1 shows the number of positions, where the particular amount of background counts are detected. In order to get the respective count rate, this number is divided by the exposure time of the survey at this position. The exposure time is taken from the exposure map given in Sect. 1.2. By calculating the mean value, the resulting background rate  $c_b$  is 0.001202 counts per second. As this is just an assessment, the uncertainty is neglected.

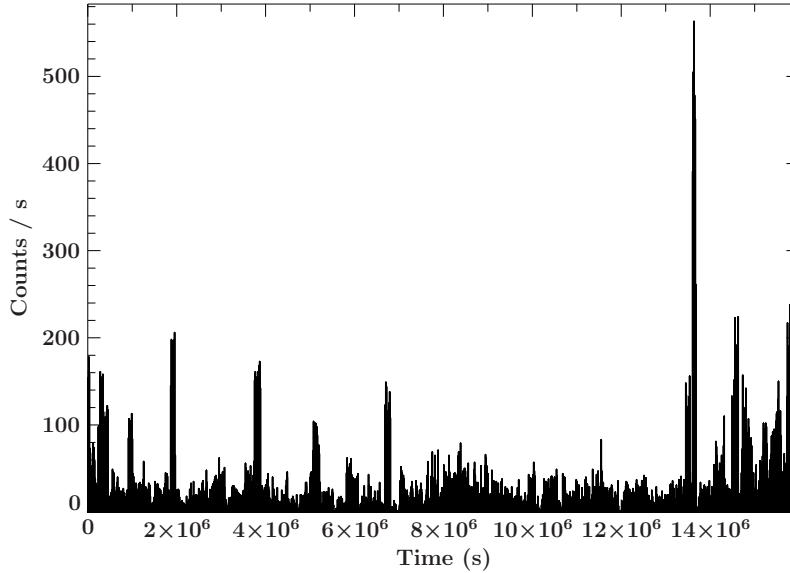


Figure 4.3: The detektor light curve binned in 50 seconds

Number of counts	Number of positions
0	773
1	191
2	31
3	4
4	1

Table 4.1: The number of positions, where the particular amount of background counts are detected

## 4.1.2 Light curve extraction

In order to make conclusions about the performance of eROSITA and to compare the input with the output, the results of the simulation have to be analysed. This is why the light curve of the each source has to be extracted from the event file. This is realised by looping over the positions stored in the source catalogue. This is possible, as it is about sources, whose positions are known.

1. Find the events, which are within a defined area around the position. The area was assumed with a radius of 40 arcsec again, as this is the magnitude of the PSF.
2. The determined events are stored in a new FITS file named after its position to distinguish between the particular files.
3. Makelc is utilised with its input/output file, the length of the light curve and its time resolution. The length was set to  $1.6 \cdot 10^7$  seconds, in order to guarantee that the whole exposure time is taken into account. The time resolution is set to 1 second, as the source is only seen for about 25 to 60 seconds.
4. Determine the absolute counts of each light curve detected during the whole exposure time.
5. As already mentioned, the source is only seen for a short period of time compared to the  $1.6 \cdot 10^7$  seconds. Thus each count entry equal zero is discarded, in order to minimise the amount of data.

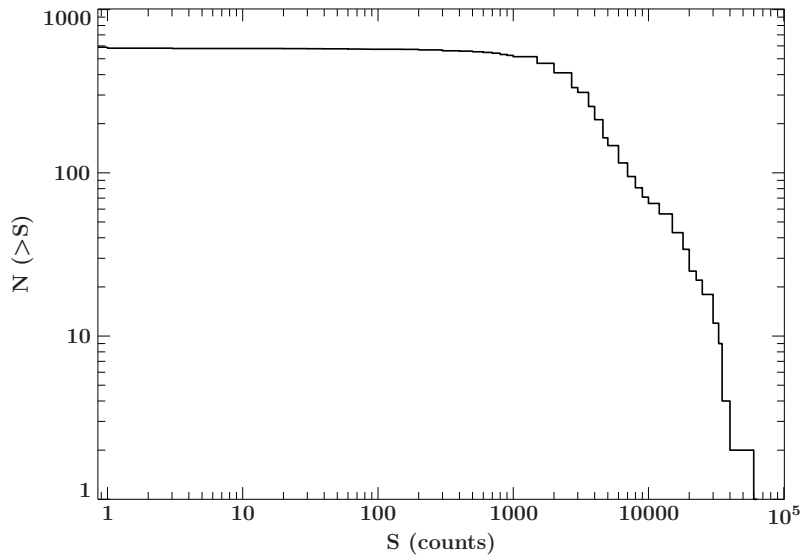


Figure 4.4: The  $\log N (>S)$  graph. It is shown the number of sources  $N$ , which have more counts than  $S$ .

6. As the plot routine, which will be used later on, interpolates linear between two data points, one has to add count entries equal zero right before and after a continuous set of entries. Otherwise, the interpolation would lead to counts within eROSITA's blind time.

Fig. 4.4 shows a  $N (> S)$  plot for all sources in the source catalogue.  $N$  is the amount of sources and  $S$  is the amount of counts. Hence the plot shows the number of sources  $N$ , which have more counts than  $S$ . Unfortunately, the data for low source counts are difficult to see, due to this representation. In total, there are 8 sources, which have 0 counts, and 3 sources, which have 1 count. It has to be reminded of the fact that 2 sources can not have any counts, as their input light curves are supplemented with zeros.

### Source detection

As mentioned in Sect. 2, it is meaningful to give an estimation for the number of sources eROSITA will be able to see, due to its special all sky survey (Sect. 1.2) and the time variability of the sources. For this reason, sources have to be detectable with a sufficient significance. As the absolute counts for each source have already been computed, the next step is the comparison with the expectation value of particular background counts. Hence the result of the assessment for the background counts (Sect. 4.1.1) is taken and has to be synchronised with the varying exposure time dependent on the source's position in the sky. As  $c_b$  is the background rate for the same amount of area, which is used for the light curve extraction, the product of  $c_b$  with the particular exposure time of the position should be a wise appraisal for the respective background counts  $C_b$ . The exposure time is taken from the exposure map in Sect. 1.2 again. The next step is the determination of the significance of the particular sources detection. It is calculated with (Bradt, 2004):

$$\text{Significance} = \frac{S}{\sigma_S} = \frac{S}{\sqrt{S + 2C_b}} \quad (4.3)$$

$S$  are the absolute detected counts of the source and  $C_b$  are the expected background counts. Except for the 11 sources with 1 or 0 counts mentioned before, all sources are detected at least with a  $4.3\sigma$  significance. Hence in total 578 of 587 sources are detected with a sufficient high significance, as two light curves are supplemented with zeros.

### 4.1.3 Comparison between the ASM- and eROSITA counts

Until now, only the output of the simulation was considered and evaluated. The next step is the examination how well the input fits to the output, which was already evaluated partly, by contemplating the input counts with the counts detected with the simulation. Thus a loop over each extracted light curve is performed. It is made one calculation for each interval  $[t_{ii}, t_{ii+1}]$  of the light curve delimited by a count entry equal zero on both sides. The intervals, in which every count entries is equal zero are discarded for this computation. These intervals occur because of the sixth step of the loop explained in Sect. 4.1.2. For the considered intervals the time difference  $t_{\text{Dif}}$  from  $t_{ii}$  and  $t_{ii+1}$  is determined with:

$$t_{\text{Dif}} = t_{ii+1} - t_{ii} \quad (4.4)$$

This is used to compute the count rate  $c_{\text{eRO}}$  for each particular interval of eROSITA with:

$$c_{\text{eRO}} = \frac{\sum_{j=ii}^{ii+1} C_j}{t_{\text{Dif}}} \quad (4.5)$$

$C_j$  are the respective counts in each one second interval. So one get a number between 0 and 418 data points for each source. Actually, one would expect as many data points as amount of times the source pass through the detector's FOV. However, for faint sources there are only detected few counts, thus there are many one second intervals, wherein you do not have any counts. As the algorithm takes each interval between two count entries equal zero, this explains the high amount of data points. On the other side you do not have any data points, if the source is not detected at all. It has to be mentioned that this algorithm produces a slight mistake, as the lowest possible count rate which can be detected is 1 count per second. More information about this mistake is given in Sect. 4.2.

In order to compare these results with the ASM data, the particular time of measurement  $t_{\text{MES}}$  is determined:

$$t_{\text{Mes}} = \frac{t_{ii+1} + t_{ii}}{2} \quad (4.6)$$

As the input light curves only have one data point every 90 seconds at its best, the particular  $t_{\text{MES}}$  is arranged between two data points of the ASM. Hence you have to find these two data points  $(T_1, f_1)$  respectively  $(T_2, f_2)$ , which enclose  $t_{\text{MES}}$ , in order to interpolate linear between these.  $T_1$  and  $T_2$  is the particular time of the data point and  $f_1$  and  $f_2$  is the particular flux of the data point in mCrab, as the count rates of the light curves are converted to the particular flux in Sect. 3.2.1.

$$f_{\text{Mes}} = f_1 + \frac{f_2 - f_1}{T_2 - T_1} \cdot (t_{\text{MES}} - T_1) \quad (4.7)$$

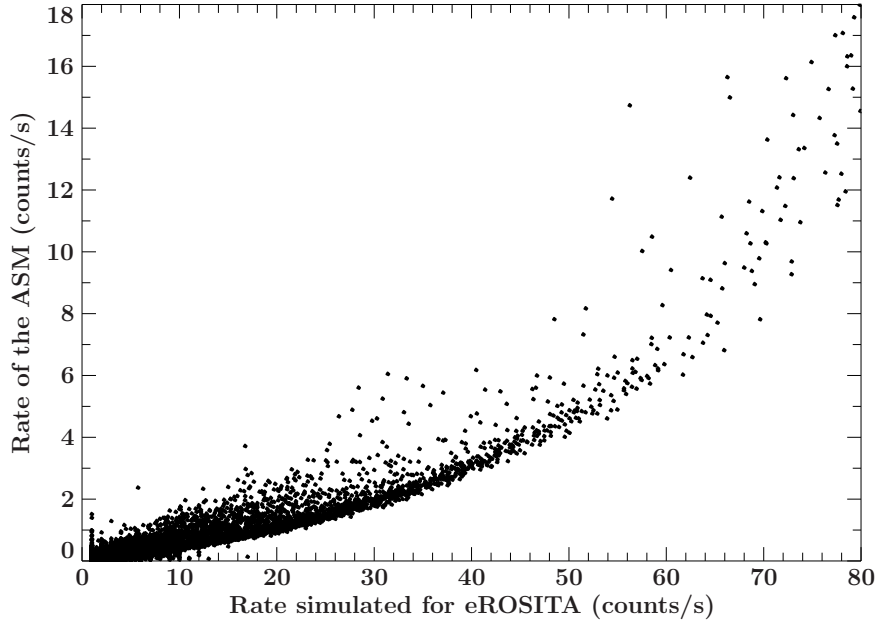


Figure 4.5: ASM rates via eROSITA rates specified in counts/s

ASM rate (counts/s)	eROSITA rate (counts/s)
907.57	122.00
1079.12	101.20
1079.18	138.33
1079.28	106.00
1125.27	98.00

Table 4.2: Pairs of data that show the pileup effect. These data are taken from the source SCO X-1, a bright low mass X-ray binary

Afterwards the flux of the ASM is converted to the particular count rate, in order to guarantee a better comparison.

$$c_{\text{ASM}} = f_{\text{Mes}} \cdot 0.075 \frac{\text{counts} \cdot \text{cm}^2}{\text{s}^2 \cdot \text{erg}} \quad (4.8)$$

Fig. 4.5 shows the plot of the ASM rates via the eROSITA rates.

The trend shows, just like expected, a linear correlation for low rates. Ideally, a line through origin is expected and the gradient defines the conversion factor between ASM counts per second and eROSITA counts per second. In actuality, a shift to ASM rates higher than expected can be seen especially for high rates. This is caused by the pileup effect (Sect. 3.4.3) for bright sources. In this case eROSITA can not distinguish between incoming photons and summarises several photons to one during the read-out cycle. For this reason, the plot seen in Fig. 4.5 is limited to low rates because there are some data point pairs with immense crucial pileup. Table 4.2 gives an example for a source with intense pileup. More precisely, these data point pairs belong to the source SCO X-1, a bright neutron star binary with  $\text{RA} = 244.98^\circ$  and  $\text{DEC} = -15.64^\circ$ .

### Comparison between input light curves and simulated light curves

So far, one just made the comparison of the rates in general. The next step is the comparison between the input and output light curves. This is why a loop over each source is performed. At first, the time of the first time eROSITA detects the source

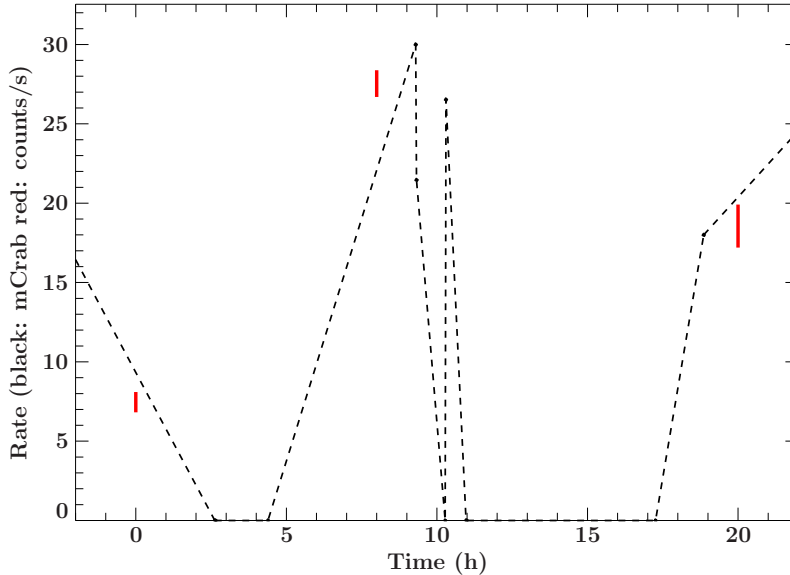


Figure 4.6: Comparison of the light curves of the source IGRJ17098-3626 positioned at RA = 257.44° and DEC = -36.47°; black: the rate of the ASM specified in mCrab; red: the rate of eROSITA with its error bars specified in counts per second

is taken from the data calculated before. Afterwards, both light curves are shifted in time by this determined time. In order to guarantee a better comparison, the units of the input and simulation time are converted into hours, as each measurement of eROSITA is performed every 4 hours. Before plotting the data the errors of the simulation data have to be determined. As the counts are Poisson distributed, the uncertainties of the total counts  $e_C$  are calculated by taking the root of the total counts  $C_j$  of each measurement:

$$e_C = \sqrt{C_j} \quad (4.9)$$

As this is the uncertainty of the total counts and the rates will be plotted, the error of the rates must be calculated with:

$$e_c = \frac{e_C}{t_{\text{Dif}}} \quad (4.10)$$

Thus the particular rates of the simulation with its error bars  $c_S$  are defined as:

$$c_S = \frac{C_j}{t_{\text{Dif}}} \pm e_c \quad (4.11)$$

In Fig. 4.6 the source positioned at RA = 257.44° and DEC = -36.47° is shown, as this represents the typical result for count rates within the linear correlation. The black data points represent the ASM data specified in mCrab, the dashed line represent the linear interpolation between two data points. The red data points represent the eROSITA rates with their error bars specified in counts per second. As the input light curve is equal zero for  $t = 4, 12,$  and  $16$  hour, no eROSITA counts are detected in these periods.

## 4.2 Discussion

The results show that 587 of 589 sources can be seen with a sufficient significance, thus 11 sources are not detected. It has to be taken into account that 2 of the 11

sources are not-detectable, as their light curves were supplemented with zeros. Thus 578 of 587 sources are detectable with a high significance. However, there are some weaknesses and simplifications made in this thesis, which have to be mentioned. At first, one only analysed the transient characteristics regarding the luminosity. As a matter of fact, the spectra have transient characteristics too. Another simplification made in this thesis is that only one telescope is simulated for half a year, although eROSITA has seven telescopes, which will perform eight surveys lasting half a year each. By performing a complete simulation with seven telescopes and eighth all sky surveys, a comparison between the different telescopes and all sky scans could be made. Furthermore, the simulation was actually performed for slightly more than half a year with the consequence that some sources are detected 2 times with eROSITA. This has an impact on the total count plot (Fig. 4.4), as one actually performs 2 all sky surveys for some sources. Furthermore, no algorithm or criterion was developed to detect transient sources by just using the event file. One just looked at the positions the sources were expected, as these are stored in the SIM-PUT catalogue used as input. Another important point to be mentioned is a fact concerning the calculation of the eROSITA rates in Sect. 4.1.3. As the algorithm used in this thesis only considers the time wherein arriving photons are detected, the rates for faint sources are incorrect. As a consequence of this algorithm, the minimal count rate, which can be detected, is 1 count per second. In actuality, eROSITA is able to detect much fainter sources. For example, there is the possibility, that eROSITA looks at a source for, e.g., 10 seconds but only 1 count is measured for this time. With the algorithm used in this thesis, the measured count rate is 1 count per second, whereat the correct count rate is 0.1 counts per second. This aspect especially affects the count rates of faint sources. In order to improve the algorithm, the actual exposure time during each period of time the source is within eROSITA's FOV has to be calculated. This period of time is called good time interval. Finally, the quality of the data in the source catalogue has to be noted. The ASM has only a rough time resolution and relatively bad sensitivity compared to eROSITA. Hence it is not possible to make a statement about the results of the simulation regarding the pulsations from milliseconds to seconds, which many sources are expected to show. As it is interpolated linear between two data points the sources can not show these pulsations, although they occur in reality. The last point to be appended caused by the restricted input data is that you can not analyse the behaviour of eROSITA concerning the detection of faint sources. In this thesis, it is only given an assessment how many bright sources eROSITA will be able to detect, as the ASM's sensitivity is about 20 mCrab, thus it only detected the brightest X-ray sources. In actuality, eROSITA is expected to detect thousands of new galaxy clusters, AGNs and other faint sources. Hence an assessment how many of these sources can be seen would be interesting. In order to deal with this task, a better algorithm compared with an additional simulation for fainter sources with luminosities with the magnitude of eROSITA's minimal sensitivity could be performed.

# Bibliography

- A. van Riper, K., Epstein, R., 1993, *SCIENCE*, 262
- Bradt, H., 2004, *Astronomy Methods - A Physical Approach to Astronomical Observations*, Cambridge: Cambridge University Press
- Friedrich, P., 2013, *Scientific near real-time analysis software for eROSITA*, Diploma thesis, Universität Erlangen
- Giles, A.B., Jahoda, K., Swank, J.H., Zhang, W., 1995, *Publications of the Astron. Soc. of Australia*, 12, 219
- Harding, A.K., 2013, *Frontiers of Physics*, 8, 679
- Lochner, J.C., Remillard, R.A., 1995, in *American Astronomical Society Meeting Abstracts*, Vol. 27, *Bulletin of the American Astronomical Society*, 1418
- Mauche, C.W., Liedahl, D.A., Akiyama, S., Plewa, T., 2008, in M. Axelsson (ed.), *American Institute of Physics Conference Series*, Vol. 1054, *American Institute of Physics Conference Series*, 3
- Mori, K., Burrows, D.N., Hester, J.J., et al., 2004, *Astrophysical Journal*, 609, 186
- Nowak, M.A., Wilms, J., Hanke, M., et al., 2012, *Mem. Societa Astronomica Italiana*, 83, 202
- Pence, W.D., Chiappetti, L., Page, C.G., et al., 2010, *Astronomy and Astrophysics*, 524, A42
- Predehl, P., 2012, in *Space Telescopes and Instrumentation 2012: Ultraviolet to Gamma Ray*, Vol. 8443, *Proceedings of the SPIE*, 84431R
- Predehl, P., Hasinger, G., Böhringer, H., et al., 2006, in *Society of Photo-Optical Instrumentation Engineers (SPIE) Conference Series*, Vol. 6266, *Proceedings of the SPIE*, 62660P
- Savonije, G.J., 1978, *Astronomy and Astrophysics*, 62, 317
- Schmid, C., 2008, *Simulation of the imaging and detection properties of the eROSITA experiment on Spectrum-X-Gamma*, Diploma thesis, Universität Erlangen
- Schmid, C., 2012, *X-ray Telescopes in the Digital Lab: Instrument Performance Simulations*, Ph.d. thesis, Universität Erlangen

- Seward, F.D., Charles, P.A., 1995, Exploring the X-Ray Universe -, Cork: CUP Archive
- Tenzer, C., Warth, G., Kendziorra, E., A., S., 2010, Proceedings of the SPIE, 7742
- Wen, L., Levine, A.M., Corbet, R.H.D., Bradt, H.V., 2006, Astrophysical Journal, 163, 372
- Wilms, J., Allen, A., McCray, R., 2000, Astrophysical Journal, 542, 914
- Wolter, H., 1952, Annalen der Physik

# Acknowledgements

First of all, I would like to thank Jörn Wilms who offered this great subject to me and who always helped me when problems occurred.

Subsequently, I would like to thank Thorsten Brand and especially Thomas Dauer who introduced me to SIXTE and helped me with problems in ISIS.

Furthermore, my gratitude belongs to Ralf Ballhausen who has always been there for me concerning all kinds of problems with ISIS or linux in general.

I also thank Tobias Hain who shared the first steps in SIXTE with me.

Finally, I would like to thank the whole staff of the Remis observatory for the great ambience.

# Selbständigkeitserklärung

Hiermit bestätige ich, dass ich diese Arbeit selbstständig und nur unter Verwendung der angegebenen Hilfsmittel angefertigt habe.

---

Ort, Datum

---

Unterschrift